This is an accepted manuscript of an article published by Elsevier in European Journal of Cell Biology (accepted 23/06/2016) available at: http://dx.doi.org/10.1016/j.ejcb.2016.06.008.

==========

The TRPM7 interactome defines a cytoskeletal complex linked to neuroblastoma progression

Jeroen Middelbeek[1]*, Kirsten Vrenken[1]*, Daan Visser[2], Edwin Lasonder[3,4] (present address), Jan Koster[5], Kees Jalink[2], Kristopher Clark[1,6] (present address)‡ and Frank N. van Leeuwen[1‡]

[1]Laboratory of Pediatric Oncology and [3] Centre for Molecular and Biomolecular Informatics, Radboud Institute for Molecular Life Sciences, Radboudumc, P.O. Box 9101, 6500 HB, Nijmegen, The Netherlands
[2]Division of Cell Biology I, The Netherlands Cancer Institute (NKI-AVL), Plesmanlaan 121, 1066 CX, Amsterdam, The Netherlands
[4]School of Biomedical & Healthcare Sciences, Plymouth University Peninsula Schools of Medicine and Dentistry, Portland Square, Plymouth, PL4 8AA, UK
[5]Department of Oncogenomics, Academic Medical Center, Meibergdreef 9, 1105 AZ, Amsterdam, The Netherlands
[6]Sygnature Discovery Limited, Biocity, Pennyfoot street, Nottingham, NG1 1GF, UK

* contributed equally
‡ contributed equally

***Corresponding author:**
Frank N. van Leeuwen, PhD
Laboratory of Pediatric Oncology
Radboud Institute for Molecular Life Sciences, Radboudumc
PO Box 9101, 6500 HB Nijmegen, The Netherlands
T: +31 243666203
F: +310243666352
FrankN.vanLeeuwen@radboudumc.nl

Abstract

Neuroblastoma is the second-most common solid tumor in children and originates from poorly differentiated neural crest-derived progenitors. Although most advanced stage metastatic neuroblastoma patients initially respond to treatment, a therapy resistant pool of poorly differentiated cells frequently arises, leading to refractory disease. A lack of insight into the molecular mechanisms that underlie neuroblastoma progression hampers the development of effective new therapies for these patients.

Normal neural crest development and maturation is guided by physical interactions between the cell and its surroundings, in addition to soluble factors such as growth factors. This mechanical crosstalk is mediated by actin-based adhesion structures and cell protrusions that probe the cellular environment to modulate migration, proliferation, survival and differentiation. Whereas such signals preserve cellular quiescence in non-malignant cells, perturbed adhesion signaling promotes de-differentiation, uncontrolled cell proliferation, tissue invasion and therapy resistance. We previously reported that high expression levels of the channel-kinase TRPM7, a protein that maintains the progenitor state of embryonic neural crest cells, are closely associated with progenitor-like features of tumor cells, accompanied by extensive cytoskeletal reorganization and adhesion remodeling. To define mechanisms by which TRPM7 may contribute to neuroblastoma progression, we applied a proteomics approach to identify TRPM7 interacting proteins. We show that TRPM7 is part of a large complex of proteins, many of which function in cytoskeletal organization, cell protrusion formation and adhesion dynamics. Expression of a subset of these TRPM7 interacting proteins strongly correlates with neuroblastoma progression in independent neuroblastoma patient datasets. Thus, TRPM7 is part of a large cytoskeletal complex that may affect the malignant potential of tumor cells by regulating actomyosin dynamics and cell-matrix interactions.

Keywords

TRPM7
Cytoskeletal proteins
Cell adhesion
Cell protrusion
Neuroblastoma progression

Introduction

Neuroblastoma is one of the most common malignancies in childhood and responsible for 12% of cancer associated deaths in children (Maris, 2010; Morgenstern et al., 2013). A lack of insight into the molecular mechanisms that contribute to neuroblastoma progression hampers the development of effective new therapies (Maris, 2010; Morgenstern et al., 2013; Schramm et al., 2015). Neuroblastoma is an embryonic tumor derived from pluripotent cells of the neural crest. The neural crest is a heterogeneous cell population that arises at the borders of the neuro-ectoderm during early embryogenesis. Neural crest cells exhibit adaptive plasticity, i.e. the ability of phenotypic switching to allow cell-fate changes when necessary (Prasad et al., 2012; Thiery et al., 2009; Yang and Weinberg, 2008). These cell fate decisions are largely controlled by cues from the tissue microenvironment. In addition to growth factors and other soluble cues, cellular processes such as proliferation, migration and differentiation are directed by the mechanical crosstalk between cells and their microenvironment (Geiger et al., 2009; Kim et al., 2014; Paszek et al., 2005; Wirtz et al., 2011). The physical cross-talk between a cell and the surrounding tissue is mediated by cell adhesion sites and cellular protrusions such as lamellipodia and filopodia. These structures constantly probe the cellular microenvironment for chemical and mechanical cues, and signal to control cytoskeletal dynamics and gene expression. Whereas such signals preserve cellular quiescence in non-malignant cells, perturbed adhesion signaling promotes de-differentiation, uncontrolled cell proliferation, tissue invasion and therapy resistance (Eke et al., 2012; Kim et al., 2012; Matsushima and Bogenmann, 1992; Ou et al., 2012; Sloan et al., 2006; White et al., 2006; Wirtz et al., 2011). Indeed, several studies indicate that altered cell-matrix interactions significantly contribute to neuroblastoma pathogenesis (Feduska et al., 2013; Lee et al., 2012; Megison et al., 2013; Meyer et al., 2004; Molenaar et al., 2012; Yoon and Danks, 2009).

Members of the mammalian TRP channel family play a central role in mechano-signaling (Clark et al., 2008c; Lin and Corey, 2005; Numata et al., 2007a, b; Oancea et al., 2006; Orr et al., 2006). Localized within mechano-sensory structures such as cell adhesions, channel opening is induced by membrane stretch and/or cytoskeletal tension. The resulting changes in local ion concentrations trigger cytoskeletal responses and regulate gene expression. The importance of these channels during embryonic development, tissue homeostasis and tumor progression is now widely recognized (reviewed in (Clark et al., 2008c; Delmas and Coste, 2013; Kuipers et al., 2012; Vrenken et al., 2015)). For instance, TRPM7, a calcium permeable TRP-channel with a functional C-terminal kinase domain that localizes to cell adhesion sites, is required during the development of embryonic organ systems in mice, zebrafish and *Xenopus*, and maintains stemcell-like features of neural crest progenitor cells (Jin et al., 2008; Jin et al., 2012; Visser et al., 2014). Consistently, we identified TRPM7 as a regulator of cell mechanics that drives the malignant behavior of neuroblastoma cells by activating developmental programs *in vitro* and *in*

vivo (Middelbeek et al., 2015). Recent reports have confirmed the association between high *TRPM7* expression and cancer progression in other tumor types, including pancreatic, nasopharyngeal, breast and prostate cancer (Chen et al., 2014; Middelbeek et al., 2012; Rybarczyk et al., 2012; Sun et al., 2013). Although little is known about the molecular mechanism by which TRPM7 promotes tumor progression, we previously established that TRPM7 regulates cellular tension through Ca^{2+}- and kinase-dependent interactions with the actomyosin cytoskeleton (Clark et al., 2006; Clark et al., 2008a; Clark et al., 2008b). Based on the presence of TRPM7 in adhesion structures and because TRPM7 can be activated by mechanical stress, this cation channel may act to control cytoskeletal dynamics and downstream signaling pathways in response to mechanical cues, to promote the progenitor-like features of neuroblastoma cells (Clark et al., 2006; Numata et al., 2007a, b; Oancea et al., 2006; Su et al., 2006).

By performing mass-spectrometry on TRPM7 immune complexes, obtained from N1E-115 neuroblastoma cells expressing HA-tagged TRPM7, we set out to identify the TRPM7 interactome in neuroblastoma cells. We show that TRPM7 is part of a large cytoskeletal protein complex which mostly contains proteins involved in cell protrusion dynamics and adhesion formation. By combining a comprehensive literature study with microarray-based gene expression analysis, we demonstrate that ~55% of the TRPM7 interactors are associated with cancer progression and metastasis formation. Moreover, a number of these components accurately predicts neuroblastoma disease outcome in three independent neuroblastoma patient cohorts. Together, our results provide further insight into the close interactions between TRPM7 and the actomyosin cytoskeleton, and suggest a regulatory role for the TRPM7 interactome in cancer progression.

Results & Discussion

TRPM7 associates with a protein complex that controls cytoskeletal organization

To define the mechanism by which TRPM7 contributes to neuroblastoma progression, we identified proteins in complex with TRPM7 using a proteomic approach (**Fig. 1A**). The TRPM7 complex was purified by immunoprecipitation from mouse N1E-115 neuroblastoma cells made to express TRPM7-HA (Clark et al., 2006). Associated proteins were resolved by SDS-PAGE. Silver staining of the gels revealed several proteins that were strongly enriched in the TRPM7 fraction (**Fig. 1B**). Proteins present in the control and TRPM7 immunoprecipitations were identified by nano liquid chromatography tandem mass spectrometry (LC-MS/MS) and proteins were considered to specifically interact with TRPM7 when corresponding peptides were exclusively detected in the TRPM7 fraction (TRPM7 IP exclusive), or when peptides were detected in both control and TRPM7 fractions but showing an iBAQ ratio between TRPM7 and control fraction greater than 10 (enriched). This analysis led to the identification of 251 proteins of which 64 appear to be in a complex with TRPM7 (**Table 1 & S1**). Proteins were classified according to Gene Ontology (GO) annotation for molecular function, cell component and biological process. A

distribution of GO terms between the control and TRPM7 fractions showed that the TRPM7 protein complex is specifically enriched for proteins involved in the organization and biogenesis of the actomyosin cytoskeleton (**Fig. 1C**). This set of proteins includes conventional myosin II and several non-conventional myosins (myosins I, V and VI) as well as proteins regulating actin dynamics such as components of the Arp2/3 complex, F-actin capping proteins, drebrin, tropomyosins, tropomodulin, gelsolin and cofilin. Moreover, a group of structural proteins involved in cross-linking and scaffolding the cytoskeleton, including α-actinin4 and plectin, was also present (**Table 1**).

We were able to confirm a substantial number of interactions between TRPM7 and its cytoskeletal interactors by immunoprecipitation and Western blotting (**Fig. 2**). The interactions between TRPM7 and the actomyosin cytoskeleton appear to be highly specific. First of all, none of the interactors were found in significant quantities in control immunoprecipitations (**Table S1**). Moreover, actin-binding proteins such as α-actinin1, cortactin, talin and vinculin, which are abundantly expressed in these cells and thus likely contaminants in immunoprecipitations, were not detected either by mass spectrometry or Western blotting (**Table S1, Fig. 2**). Finally, the detection of myosin IIA, IIB and IIC heavy chain, known substrates of the TRPM7 kinase domain (Clark et al., 2006; Clark et al., 2008a; Clark et al., 2008b), further validates our proteomics approach. Note that the interaction between TRPM7 and the cytoskeleton is not restricted to ectopically expressed TRPM7-HA, as we previously showed that endogenous TRPM7 also interacts with the actomyosin cytoskeleton (Clark et al., 2006).

The TRPM7 interactome is a macromolecular complex involved in cell adhesion and protrusion formation

We previously showed that TRPM7 is enriched in invadosome-type adhesions where it may aid in the assembly of such structures (Clark et al., 2006). Invadosomes are highly dynamic, matrix degrading adhesion structures that act as mechanosensory devices by detecting rigidity and topography of the substratum (Gimona et al., 2008; Linder and Wiesner, 2015; Linder et al., 2011). Consistent with a role for TRPM7 in mechanical regulation of cytoskeletal dynamics, a significant number of TRPM7 interactors are known constituents of either the invadosome core, such as F-actin, F-actin capping proteins, Arp2/3, gelsolin, cofilin, or the ring, such as nonmuscle myosin IIA and tropomyosin (Gimona et al., 2008; Linder, 2007; Linder et al., 2011) (**Table 1**). Moreover, the 'TRPM7 interactome' comprises previously unknown invadosome components, including drebrin, myosin IIB and IIC, myosin Va, α-actinin4 and SIPA1-L1/SPAR1 (**Fig. 3**). The observation that many TRPM7 interactors localize to these defined cellular structures supports the specificity of our proteomics approach.

Consistent with the fact that invadosomes are actin-based protrusive structures, many of the TRPM7 interactors are known to regulate the dynamic formation of cellular protrusions such

as filopodia, neuronal growth cones, dendritic spines and podocytes (Goel et al., 2005; Goswami and Hucho, 2008; Kuipers et al., 2012). For instance, the 'TRPM7 interactome' component calmodulin is a calcium sensor that can activate the serine/threonine phosphatase calcineurin (Li, 1984). Calcineurin regulates cytoskeletal organization and neurite extension by activation of the phosphatase slingshot (SSH2) and its substrate cofillin (CFL1), both of which are present in the TRPM7 interactome (Descazeaud et al., 2012; Wang et al., 2005). The vesicle carrier myosin Va links long distance microtubule-based cargo transport to short distance actin-based transport and is crucial for filopodia and neurite extension (Ali et al., 2008; Desnos et al., 2007; Wang et al., 1996). Tropomodulin 2, in turn, is an actin-regulatory protein with capping activity that regulates actin polymerization and neurite extension (Fath et al., 2011). Many other TRPM7 interacting proteins, such as myosin VI (Lewis et al., 2011), drebrin (Ishikawa et al., 1994; Majoul et al., 2007; Mercer et al., 2010), TAX1BP1 (Morriswood et al., 2007), and SIPA1-L1/SPAR1 (Pak et al., 2001), have been similarly implicated in the regulation of adhesion dynamics and cell protrusion formation. Together, these findings suggest that, as a functional complex located at sites of cell adhesion or in cellular protrusions, the TRPM7 interactome may control cytoskeletal organization in response to mechanical cues from the tissue microenvironment.

The functional implications of the interactions between TRPM7 and its cytoskeletal binding partners remain incompletely understood. We have shown in the past that inhibition of TRPM7 results in the disassembly of invadosomes (Visser et al., 2013), which suggests that activity of TRPM7 is involved in maintaining the integrity of the 'TRPM7 interactome'. This is consistent with the general notion that TRP channels act as cytoskeletal scaffolding proteins (Clark et al., 2008c; Kuipers et al., 2012). Furthermore, our earlier work revealed that TRPM7 regulates the activity non-muscle myosin II isoforms through kinase-dependent interactions with the myosin II heavy chain, promoting the assembly of invadosomes. If and how TRPM7 may affect the localization and function of other interactome components will be addressed in future studies

Components of the 'TRPM7 interactome' correlate with human neuroblastoma metastasis

A recent study by Molenaar et.al. shows that defects in genes encoding regulators of cytoskeletal dynamics strongly associate with high-risk neuroblastomas with an aggressive clinical course (Molenaar et al., 2012). An extensive literature survey demonstrated that expression of TRPM7 and many TRPM7 interactors (~55%) have been associated with disease outcome in various cancers, although only a minority of these have thus far been implicated in neuroblastoma progression (~5%) (**Table 1**). We therefore tested to what extent components of the TRPM7 interactome associate with outcome in human neuroblastoma, using microarray-based neuroblastoma gene expression datasets. The discovery dataset (Kocak - 649) contained expression profiles of 649 primary tumor biopsies, along with clinical information on overall and

relapse-free survival (Kocak et al., 2013). Probes for all validated components of the TRPM7 interactome were present on this microarray. We previously reported that TRPM7 itself associates with disease outcome in this dataset (Middelbeek et al., 2015). Additionally, mRNA expression of a substantial number of TRPM7 interactors correlate significantly with overall (33 out of 64) and relapse free survival (30 out of 64) after correction for multiple testing. We performed similar analyses using two independent validation cohorts of 88 (Versteeg-88) and 251 (Oberthuer-251) neuroblastoma patients (Geerts et al., 2010; Oberthuer et al., 2006). In the Versteeg-88 and Oberthuer-251 cohorts, respectively 14 out of 60 and 25 out of 35 TRPM7 interactors present on the array correlate significantly with disease outcome (**Table S2**). Across the three datasets, we observed striking similarities in the co-regulation of genes that associate with neuroblastoma disease progression. Expression of 18 interactors were similarly associated with disease progression in at least 2 out of 3 datasets (**Table 1**). Regulators of adhesion dynamics and cytoskeletal organization junctional plakoglobin (*JUP*), myosin light chain 6 (*MYL6*), myosin 5A (*MYO5A*), tropomodulin 2 (*TMOD2*) are amongst the interactors that correlated most significantly with disease outcome (**Fig. 4**).

The TRPM7 interactome comprises proteins that either positively or negatively associate with tumor progression. This may seem to be at odds with the notion that high TRPM7 expression is generally associated with poor disease outcome. However, TRPM7 may either positively OR negatively regulate the activity of its interactors. Similarly, the different interactors of TRPM7 may oppositely affect the aggressive features of neuroblastoma cells. Overall, these observations suggest that TRPM7 is part of a cytoskeletal complex that controls the dynamic formation and function of mechanosensory structures such as cell adhesions and cellular protrusions. This complex may function to control neural crest development in response to mechanical cues, but when deregulated it could contribute to neuroblastoma disease progression.

Concluding remarks

There is growing evidence that mammalian TRP channels form large macromolecular complexes linked to the actomyosin cytoskeleton (Clark et al., 2008c; Kuipers et al., 2012). Organization of TRP channels into large multiprotein complexes (signalplexes) may serve to localize signal transduction pathways and/or enhance the rate of signal transmission. By similarity to TRP channels in Drosophila photoreceptors (Tsunoda et al., 2001), TRPM7 may function to anchor and maintain the integrity of the complex. Additionally, TRPM7 kinase activity and ion conductance potentially modulate the activity of cytoskeletal components within the complex. A more detailed understanding of the function of the TRPM7 interactome in neuroblastoma may offer new strategies for inducing neuroblastoma differentiation and to overcome therapy resistance in the patient.

Acknowledgements

We thank the Nijmegen Proteomics Facility for usage of the LC-MS/MS equipment to carry out this study. We thank D. Clapham and O. van Tellingen for TRPM7 in pTracer-CMV and pMX-luciferase-YFP-neo, J. Klarenbeek for technical assistance, and members of the Division of Cell biology and group members for support, discussions and critical reading of the manuscript. This work was supported by KWF grants (KUN 2007-3733 and NKI 2010-4626) and KiKa (104) to KJ and FvL, and a Radboudumc PHD grant to KV

Material and Methods

Constructs and cell lines

Full length TRPM7 cDNA, cloned into LZRS-neo, was previously described (Clark et al., 2006). The recombinant protein contains an HA-tag at the C-terminus. Mouse N1E-115 neuroblastoma cells were cultured in DMEM supplemented with 10% FCS and 1% penicillin-streptomycin. N1E-115 cells stably expressing TRPM7-HA and empty vector control were generated using retroviral transduction. Transduced cells were selected by the addition of 0.8 mg/ml G418.

Immunoprecipitation

N1E-115 control and TRPM7-transduced cells were washed twice in ice-cold PBS and subsequently, lysed on ice for 30 min in a buffer containing 50 mM Tris pH 7.5, 300 mM NaCl, 1.5 mM $MgCl_2$, 0.2 mM EDTA, 0.5 mM DTT, 1% Triton X-100 and protease inhibitors. The lysate was cleared by centrifugation for 30 min at 16000 g. HA-tagged proteins were immunoprecipitated by incubating the supernatant with proteinG-sepharose beads that were blocked with 0.5 %w/v BSA and precoupled with 12CA5 monoclonal anti-HA antibodies (Sigma Aldrich). The samples were incubated on an end-over-end rotor for 3 h at 4 °C. Subsequently, the immunocomplexes were washed in MyoII lysis buffer and solubilized in Laemmli buffer.

Mass Spectrometry

1. Nano LC-MS/MS measurements

Proteins were separated by SDS-PAGE on 6% and 12% polyacrylamide gels and subsequently, detected by silver staining. Gels were sliced into pieces and digested with trypsin overnight at 37 °C. Peptide mass spectrometric experiments were performed using a nano-HPLC Agilent 1100 system connected to a 7-Tesla linear quadruple ion trap-Ion Cyclotron Resonance Fourier transform (LTQFT) mass spectrometer (Thermo Fisher). Peptides were separated on 15 cm 100 µm ID PicoTip (New Objective) columns packed with 3 µm Reprosil C18 beads (Dr. Maisch GmbH) using a 45 min gradient from 10% buffer B to 35% buffer B (80% acetonitrile in 0.5% acetic acid). Peptides eluting from the column tip were electrosprayed directly into the mass spectrometer with a spray voltage of 2.1 kV. Peptide selection and fragmentation was set by the Xcalibur 1.4 data acquisition software (Thermo Electron). The mass spectrometer was operated in the data-dependent mode to sequence the four most intense ions per duty cycle. Briefly, full-scan MS spectra of intact peptides (*m*/*z* 350–1500) with an automated gain control accumulation target value of 10^6 ions were acquired in the Fourier transform ion cyclotron resonance (FT ICR) cell with a resolution of 50000. The four most abundant ions were sequentially isolated and fragmented in the linear ion trap by applying collisionally induced dissociation using an accumulation target value of 20000 (capillary temperature, 150°C; normalized collision energy, 30%). A dynamic exclusion of ions previously sequenced within 180 s was applied. All

unassigned charge states were excluded from sequencing. A minimum of 500 counts was required for MS^2 selection.

2. Proteome data analysis

Mass spectrometry data were analyzed with the protein identification and quantification algorithms embedded in the MaxQuant /Andromeda software (Cox and Mann, 2008). Raw spectrum files were converted into peak lists for the top 6 peaks per 100 Da window. Peptides and proteins were identified by searching the peak lists against the mouse IPI database (version 3.88) supplemented with frequently observed contaminants and concatenated with reversed copies of all entries. Andromeda (Cox et al., 2011) search parameters for protein identification specified a mass tolerance of 6 ppm for the parental peptide and 0.5 Da fragmentation spectra and a trypsin specificity allowing up to 3 miscleaved sites. Carboxyamidomethylation of cysteines was specified as a fixed modification, and oxidation of methionine were set as variable modifications. The required minimal peptide length was set at 6 amino acids. We accepted peptides and proteins with a false discovery rate (FDR) better than 0.01. Label-free quantification was performed by MaxQuant with iBAQ values reflecting protein abundance (Schwanhausser et al., 2011).

3. Functional annotation of identified proteins

Validated peptides of all samples combined were remapped to mouse IPI database version 3.88 to remove protein redundancy between different samples using an in-house Perl script. Priority of redundant IPI entries was given to Swiss prot, TREMBL, and REFSEQ entries respectively for maximising Gene Ontology (GO) annotation of identified proteins. External contaminating proteins (keratins, trypsin) were excluded for further analysis. Entrez gene identifiers were obtained using the Gene Conversion ID tool of DAVID (http://david.abcc.ncifcrf.gov/). Proteins in TRPM7 and control immuniprecipitations were quantified by intensity-based absolute quantification (iBAQ) (Schwanhausser et al., 2011), and normalized with median expression values. Proteins were considered enriched in the TRPM7 immunoprecipitate when the ratio between normalized iBAQ score in TRPM7 and control immunoprecipitates was larger than 10. Subsequent GO annotation analysis was performed using the DAVID functional annotation tool. First, GO-term enrichment in both TRPM7 and control immunoprecipitates, relative to the mouse whole genome, was determined. Next, the number of proteins in TRPM7 and control immunoprecipitates, functionally annotated to the most significantly enriched terms in the categories 'molecular function', 'biological process' and 'cellular function', were compared. Statistical significance was calculated using the fisher exact test and corrected for multiple testing (FDR).

Western blotting

Proteins were separated by SDS-PAGE and transferred to nitrocellulose. Subsequently, proteins were detected by immunoblotting using anti-α-actinin1 (1:1000; Sigma), anti-cortactin (1:500; (Schuuring et al., 1993)), anti-talin (1:500; Sigma), anti-vinculin (1:2000; Sigma), anti-myosin IIA (1:1000; Sigma), anti-myosin IIB (1:1000; Sigma), anti-myosin IIC (1:1000; (Golomb et al., 2004)), anti-drebrin (1:1000, Progene), anti-p116^{Rip} (1:2000, (Mulder et al., 2004)), anti-α-actinin4 (1:500, K. Cho), and anti-tropomodulin2 (1:1000, Abcam) followed by HRP-conjugated secondary antibodies (1:5000; Dako). Antibody-reactive bands were visualized by treating the blots with ECL (Amersham) followed by autoradiography.

Microscopy

N1E-115/TRPM7 cells were seeded on glass coverslips and serum starved (0.1% FCS) overnight prior to stimulation with 200nM bradykinin for 15 min. Cells were fixed with 4% paraformaldehyde in PBS for 10 minutes at room temperature and subsequently permeabilized with 0.1% triton X-100 in PBS for 3 minutes. Antibodies were used to reveal the presence of anti-myosin IIA (1:100; BTI), anti-myosin IIB (1:100, Sigma), anti-myosin IIC (1:100, (Golomb et al., 2004)), anti-drebrin (1:100, Progene), anti-p116^{Rip} (1:200, (Mulder et al., 2004)), anti-α-actinin4 (1:200, K. Cho), anti-tropomodulin2 (1:100, Abcam) and alexa488-conjugated secondary antibodies (1:1000; Molecular Probes). As no antibodies were available against myosin V and SIPA1-L1, GFP- and Myc-tagged proteins, respectively, were introduced into N1E-115/TRPM7 cells. Transfections were carried out using Fugene HD Transfection Reagent (Roche Applied Science) according to manufacturer's protocol. F-actin was detected using Aleaxa-568 phalloidin (1:100; Molecular Probes). Cells were viewed using a Leica TCS SP5 confocal microscope.

Microarray-based patient dataset analysis

Both the discovery cohort (Kocak-649) and validation cohorts (Versteeg-88 and Oberthuer-251) have been previously described and microarray based expression data are publically available). Statistical analyses were performed using R2 genomics analysis and visualization platform, developed at the department of Oncogenomics, Academic Medical Center in the University of Amsterdam (http://r2.amc.nl). For each gene that was analyzed, discovery and validation cohorts were dichotomized based on an optimal cut-off value (Kaplanscan). In short, the optimal threshold was determined as follows: (1) patient samples were sorted, based on normalized expression of the gene of interest; (2) for all possible thresholds, significance of the correlation with disease outcome (overall survival, recurrence free survival or bone/bonemarrow metastasis free survival) was calculated using the log-rank test; (3) the best performing threshold is used as cut-off value to dichotomize the cohort. To correct for multiple testing, *p*-values were Bonferoni

corrected. Survival curves were visualized by Kaplan-Meier plots, using overall survival as endpoints, and compared using log-rank tests.

Literature survey

Association of TRPM7 interactome components with cancer progression was evaluated by an online Pubmed search, using Gene ID and cancer, tumor or metastasis as search terms, followed by hand screening of titles, abstracts and full text articles. Genes were considered cancer-associated when shown to correlate with patient outcome in microarray-based gene expression profiles or when differential expression in tumor cell models affects tumorigenesis *in vitro* or *in vivo*.

References

Ali, M.Y., Lu, H., Bookwalter, C.S., Warshaw, D.M., Trybus, K.M., 2008. Myosin V and Kinesin act as tethers to enhance each others' processivity. Proc Natl Acad Sci U S A 105, 4691-4696.

Chen, J.P., Wang, J., Luan, Y., Wang, C.X., Li, W.H., Zhang, J.B., Sha, D., Shen, R., Cui, Y.G., Zhang, Z., Zhang, L.M., Wang, W.B., 2014. TRPM7 promotes the metastatic process in human nasopharyngeal carcinoma. Cancer Lett.

Clark, K., Langeslag, M., van Leeuwen, B., Ran, L., Ryazanov, A.G., Figdor, C.G., Moolenaar, W.H., Jalink, K., van Leeuwen, F.N., 2006. TRPM7, a novel regulator of actomyosin contractility and cell adhesion. EMBO J 25, 290-301.

Clark, K., Middelbeek, J., Dorovkov, M.V., Figdor, C.G., Ryazanov, A.G., Lasonder, E., van Leeuwen, F.N., 2008a. The alpha-kinases TRPM6 and TRPM7, but not eEF-2 kinase, phosphorylate the assembly domain of myosin IIA, IIB and IIC. FEBS Lett 582, 2993-2997.

Clark, K., Middelbeek, J., Lasonder, E., Dulyaninova, N.G., Morrice, N.A., Ryazanov, A.G., Bresnick, A.R., Figdor, C.G., van Leeuwen, F.N., 2008b. TRPM7 regulates myosin IIA filament stability and protein localization by heavy chain phosphorylation. J Mol Biol 378, 790-803.

Clark, K., Middelbeek, J., van Leeuwen, F.N., 2008c. Interplay between TRP channels and the cytoskeleton in health and disease. Eur J Cell Biol 87, 631-640.

Cox, J., Mann, M., 2008. MaxQuant enables high peptide identification rates, individualized p.p.b.-range mass accuracies and proteome-wide protein quantification. Nat Biotechnol 26, 1367-1372.

Cox, J., Neuhauser, N., Michalski, A., Scheltema, R.A., Olsen, J.V., Mann, M., 2011. Andromeda: a peptide search engine integrated into the MaxQuant environment. J Proteome Res 10, 1794-1805.

Delmas, P., Coste, B., 2013. Mechano-gated ion channels in sensory systems. Cell 155, 278-284.

Descazeaud, V., Mestre, E., Marquet, P., Essig, M., 2012. Calcineurin regulation of cytoskeleton organization: a new paradigm to analyse the effects of calcineurin inhibitors on the kidney. J Cell Mol Med 16, 218-227.

Desnos, C., Huet, S., Darchen, F., 2007. 'Should I stay or should I go?': myosin V function in organelle trafficking. Biol Cell 99, 411-423.

Eke, I., Deuse, Y., Hehlgans, S., Gurtner, K., Krause, M., Baumann, M., Shevchenko, A., Sandfort, V., Cordes, N., 2012. beta(1)Integrin/FAK/cortactin signaling is essential for human head and neck cancer resistance to radiotherapy. J Clin Invest 122, 1529-1540.

Fath, T., Fischer, R.S., Dehmelt, L., Halpain, S., Fowler, V.M., 2011. Tropomodulins are negative regulators of neurite outgrowth. Eur J Cell Biol 90, 291-300.

Feduska, J.M., Garcia, P.L., Brennan, S.B., Bu, S., Council, L.N., Yoon, K.J., 2013. N-glycosylation of ICAM-2 is required for ICAM-2-mediated complete suppression of metastatic potential of SK-N-AS neuroblastoma cells. BMC Cancer 13, 261.

Geerts, D., Koster, J., Albert, D., Koomoa, D.L., Feith, D.J., Pegg, A.E., Volckmann, R., Caron, H., Versteeg, R., Bachmann, A.S., 2010. The polyamine metabolism genes ornithine decarboxylase and antizyme 2 predict aggressive behavior in neuroblastomas with and without MYCN amplification. International journal of cancer 126, 2012-2024.

Geiger, B., Spatz, J.P., Bershadsky, A.D., 2009. Environmental sensing through focal adhesions. Nat Rev Mol Cell Biol 10, 21-33.
Gimona, M., Buccione, R., Courtneidge, S.A., Linder, S., 2008. Assembly and biological role of podosomes and invadopodia. Curr Opin Cell Biol 20, 235-241.
Goel, M., Sinkins, W., Keightley, A., Kinter, M., Schilling, W.P., 2005. Proteomic analysis of TRPC5- and TRPC6-binding partners reveals interaction with the plasmalemmal Na(+)/K(+)-ATPase. Pflugers Arch 451, 87-98.
Golomb, E., Ma, X., Jana, S.S., Preston, Y.A., Kawamoto, S., Shoham, N.G., Goldin, E., Conti, M.A., Sellers, J.R., Adelstein, R.S., 2004. Identification and characterization of nonmuscle myosin II-C, a new member of the myosin II family. J Biol Chem 279, 2800-2808.
Goswami, C., Hucho, T., 2008. Submembraneous microtubule cytoskeleton: biochemical and functional interplay of TRP channels with the cytoskeleton. FEBS J 275, 4684-4699.
Ishikawa, R., Hayashi, K., Shirao, T., Xue, Y., Takagi, T., Sasaki, Y., Kohama, K., 1994. Drebrin, a development-associated brain protein from rat embryo, causes the dissociation of tropomyosin from actin filaments. J Biol Chem 269, 29928-29933.
Iyengar, S., Farnham, P.J., 2011. KAP1 protein: an enigmatic master regulator of the genome. J Biol Chem 286, 26267-26276.
Jin, J., Desai, B.N., Navarro, B., Donovan, A., Andrews, N.C., Clapham, D.E., 2008. Deletion of Trpm7 disrupts embryonic development and thymopoiesis without altering Mg2+ homeostasis. Science 322, 756-760.
Jin, J., Wu, L.J., Jun, J., Cheng, X., Xu, H., Andrews, N.C., Clapham, D.E., 2012. The channel kinase, TRPM7, is required for early embryonic development. Proc Natl Acad Sci U S A 109, E225-233.
Kim, H.S., Kim, S.C., Kim, S.J., Park, C.H., Jeung, H.C., Kim, Y.B., Ahn, J.B., Chung, H.C., Rha, S.Y., 2012. Identification of a radiosensitivity signature using integrative metaanalysis of published microarray data for NCI-60 cancer cells. BMC genomics 13, 348.
Kim, K., Ossipova, O., Sokol, S.Y., 2014. Neural crest specification by inhibition of the ROCK/Myosin II pathway. Stem cells.
Kocak, H., Ackermann, S., Hero, B., Kahlert, Y., Oberthuer, A., Juraeva, D., Roels, F., Theissen, J., Westermann, F., Deubzer, H., Ehemann, V., Brors, B., Odenthal, M., Berthold, F., Fischer, M., 2013. Hox-C9 activates the intrinsic pathway of apoptosis and is associated with spontaneous regression in neuroblastoma. Cell death & disease 4, e586.
Kuipers, A.J., Middelbeek, J., van Leeuwen, F.N., 2012. Mechanoregulation of cytoskeletal dynamics by TRP channels. Eur J Cell Biol.
Lee, S., Qiao, J., Paul, P., O'Connor, K.L., Evers, M.B., Chung, D.H., 2012. FAK is a critical regulator of neuroblastoma liver metastasis. Oncotarget 3, 1576-1587.
Lewis, T.L., Jr., Mao, T., Arnold, D.B., 2011. A role for myosin VI in the localization of axonal proteins. PLoS Biol 9, e1001021.
Li, H.C., 1984. Activation of brain calcineurin phosphatase towards nonprotein phosphoesters by Ca2+, calmodulin, and Mg2+. J Biol Chem 259, 8801-8807.
Lin, S.Y., Corey, D.P., 2005. TRP channels in mechanosensation. Curr Opin Neurobiol 15, 350-357.
Linder, S., 2007. The matrix corroded: podosomes and invadopodia in ECM degradation. Trends Cell Biol, (in press).

Linder, S., Wiesner, C., 2015. Feel the force: Podosomes in mechanosensing. Experimental cell research.
Linder, S., Wiesner, C., Himmel, M., 2011. Degrading devices: invadosomes in proteolytic cell invasion. Annu Rev Cell Dev Biol 27, 185-211.
Majoul, I., Shirao, T., Sekino, Y., Duden, R., 2007. Many faces of drebrin: from building dendritic spines and stabilizing gap junctions to shaping neurite-like cell processes. Histochem Cell Biol 127, 355-361.
Maris, J.M., 2010. Recent advances in neuroblastoma. N Engl J Med 362, 2202-2211.
Matsushima, H., Bogenmann, E., 1992. Modulation of neuroblastoma cell differentiation by the extracellular matrix. Int J Cancer 51, 727-732.
Megison, M.L., Stewart, J.E., Nabers, H.C., Gillory, L.A., Beierle, E.A., 2013. FAK inhibition decreases cell invasion, migration and metastasis in MYCN amplified neuroblastoma. Clin Exp Metastasis 30, 555-568.
Mercer, J.C., Qi, Q., Mottram, L.F., Law, M., Bruce, D., Iyer, A., Morales, J.L., Yamazaki, H., Shirao, T., Peterson, B.R., August, A., 2010. Chemico-genetic identification of drebrin as a regulator of calcium responses. Int J Biochem Cell Biol 42, 337-345.
Meyer, A., van Golen, C.M., Kim, B., van Golen, K.L., Feldman, E.L., 2004. Integrin expression regulates neuroblastoma attachment and migration. Neoplasia 6, 332-342.
Middelbeek, J., Kuipers, A.J., Henneman, L., Visser, D., Eidhof, I., van Horssen, R., Wieringa, B., Canisius, S.V., Zwart, W., Wessels, L.F., Sweep, F.C., Bult, P., Span, P.N., van Leeuwen, F.N., Jalink, K., 2012. TRPM7 Is Required for Breast Tumor Cell Metastasis. Cancer Res 72, 4250-4261.
Middelbeek, J., Visser, D., Henneman, L., Kamermans, A., Kuipers, A.J., Hoogerbrugge, P.M., Jalink, K., van Leeuwen, F.N., 2015. TRPM7 maintains progenitor-like features of neuroblastoma cells: implications for metastasis formation. Oncotarget 6, 8760-8776.
Molenaar, J.J., Koster, J., Zwijnenburg, D.A., van Sluis, P., Valentijn, L.J., van der Ploeg, I., Hamdi, M., van Nes, J., Westerman, B.A., van Arkel, J., Ebus, M.E., Haneveld, F., Lakeman, A., Schild, L., Molenaar, P., Stroeken, P., van Noesel, M.M., Ora, I., Santo, E.E., Caron, H.N., Westerhout, E.M., Versteeg, R., 2012. Sequencing of neuroblastoma identifies chromothripsis and defects in neuritogenesis genes. Nature 483, 589-593.
Morgenstern, D.A., Baruchel, S., Irwin, M.S., 2013. Current and future strategies for relapsed neuroblastoma: challenges on the road to precision therapy. J Pediatr Hematol Oncol 35, 337-347.
Morriswood, B., Ryzhakov, G., Puri, C., Arden, S.D., Roberts, R., Dendrou, C., Kendrick-Jones, J., Buss, F., 2007. T6BP and NDP52 are myosin VI binding partners with potential roles in cytokine signalling and cell adhesion. J Cell Sci 120, 2574-2585.
Mulder, J., Ariaens, A., van den Boomen, D., Moolenaar, W.H., 2004. p116Rip targets myosin phosphatase to the actin cytoskeleton and is essential for RhoA/ROCK-regulated neuritogenesis. Mol Biol Cell 15, 5516-5527.
Numata, T., Shimizu, T., Okada, Y., 2007a. Direct mechano-stress sensitivity of TRPM7 channel. Cell Physiol Biochem 19, 1-8.
Numata, T., Shimizu, T., Okada, Y., 2007b. TRPM7 is a stretch- and swelling-activated cation channel involved in volume regulation in human epithelial cells. Am J Physiol Cell Physiol 292, C460-467.

Oancea, E., Wolfe, J.T., Clapham, D.E., 2006. Functional TRPM7 channels accumulate at the plasma membrane in response to fluid flow. Circ Res 98, 245-253.
Oberthuer, A., Berthold, F., Warnat, P., Hero, B., Kahlert, Y., Spitz, R., Ernestus, K., Konig, R., Haas, S., Eils, R., Schwab, M., Brors, B., Westermann, F., Fischer, M., 2006. Customized oligonucleotide microarray gene expression-based classification of neuroblastoma patients outperforms current clinical risk stratification. J Clin Oncol 24, 5070-5078.
Orr, A.W., Helmke, B.P., Blackman, B.R., Schwartz, M.A., 2006. Mechanisms of mechanotransduction. Dev Cell 10, 11-20.
Ou, J., Luan, W., Deng, J., Sa, R., Liang, H., 2012. alphaV integrin induces multicellular radioresistance in human nasopharyngeal carcinoma via activating SAPK/JNK pathway. PLoS One 7, e38737.
Pak, D.T., Yang, S., Rudolph-Correia, S., Kim, E., Sheng, M., 2001. Regulation of dendritic spine morphology by SPAR, a PSD-95-associated RapGAP. Neuron 31, 289-303.
Panayotis, N., Karpova, A., Kreutz, M.R., Fainzilber, M., 2015. Macromolecular transport in synapse to nucleus communication. Trends in neurosciences 38, 108-116.
Paszek, M.J., Zahir, N., Johnson, K.R., Lakins, J.N., Rozenberg, G.I., Gefen, A., Reinhart-King, C.A., Margulies, S.S., Dembo, M., Boettiger, D., Hammer, D.A., Weaver, V.M., 2005. Tensional homeostasis and the malignant phenotype. Cancer Cell 8, 241-254.
Prasad, M.S., Sauka-Spengler, T., LaBonne, C., 2012. Induction of the neural crest state: control of stem cell attributes by gene regulatory, post-transcriptional and epigenetic interactions. Dev Biol 366, 10-21.
Rybarczyk, P., Gautier, M., Hague, F., Dhennin-Duthille, I., Chatelain, D., Kerr-Conte, J., Pattou, F., Regimbeau, J.M., Sevestre, H., Ouadid-Ahidouch, H., 2012. Transient receptor potential melastatin-related 7 channel is overexpressed in human pancreatic ductal adenocarcinomas and regulates human pancreatic cancer cell migration. Int J Cancer 131, E851-861.
Schramm, A., Koster, J., Assenov, Y., Althoff, K., Peifer, M., Mahlow, E., Odersky, A., Beisser, D., Ernst, C., Henssen, A.G., Stephan, H., Schroder, C., Heukamp, L., Engesser, A., Kahlert, Y., Theissen, J., Hero, B., Roels, F., Altmuller, J., Nurnberg, P., Astrahantseff, K., Gloeckner, C., De Preter, K., Plass, C., Lee, S., Lode, H.N., Henrich, K.O., Gartlgruber, M., Speleman, F., Schmezer, P., Westermann, F., Rahmann, S., Fischer, M., Eggert, A., Schulte, J.H., 2015. Mutational dynamics between primary and relapse neuroblastomas. Nature genetics 47, 872-877.
Schuuring, E., Verhoeven, E., Litvinov, S., Michalides, R.J., 1993. The product of the EMS1 gene, amplified and overexpressed in human carcinomas, is homologous to a v-src substrate and is located in cell-substratum contact sites. Mol Cell Biol 13, 2891-2898.
Schwanhausser, B., Busse, D., Li, N., Dittmar, G., Schuchhardt, J., Wolf, J., Chen, W., Selbach, M., 2011. Global quantification of mammalian gene expression control. Nature 473, 337-342.
Sloan, E.K., Pouliot, N., Stanley, K.L., Chia, J., Moseley, J.M., Hards, D.K., Anderson, R.L., 2006. Tumor-specific expression of alphavbeta3 integrin promotes spontaneous metastasis of breast cancer to bone. Breast Cancer Res 8, R20.

Su, L.T., Agapito, M.A., Li, M., Simonson, W.T., Huttenlocher, A., Habas, R., Yue, L., Runnels, L.W., 2006. TRPM7 regulates cell adhesion by controlling the calcium-dependent protease calpain. J Biol Chem 281, 11260-11270.
Sun, Y., Selvaraj, S., Varma, A., Derry, S., Sahmoun, A.E., Singh, B.B., 2013. Increase in serum Ca2+/Mg2+ ratio promotes proliferation of prostate cancer cells by activating TRPM7 channels. J Biol Chem 288, 255-263.
Thiery, J.P., Acloque, H., Huang, R.Y., Nieto, M.A., 2009. Epithelial-mesenchymal transitions in development and disease. Cell 139, 871-890.
Tsunoda, S., Sun, Y., Suzuki, E., Zuker, C., 2001. Independent anchoring and assembly mechanisms of INAD signaling complexes in Drosophila photoreceptors. J Neurosci 21, 150-158.
Visser, D., Langeslag, M., Kedziora, K.M., Klarenbeek, J., Kamermans, A., Horgen, F.D., Fleig, A., van Leeuwen, F.N., Jalink, K., 2013. TRPM7 triggers Ca2+ sparks and invadosome formation in neuroblastoma cells. Cell Calcium 54, 404-415.
Visser, D., Middelbeek, J., van Leeuwen, F.N., Jalink, K., 2014. Function and regulation of the channel-kinase TRPM7 in health and disease. Eur J Cell Biol.
Vrenken, K.S., Jalink, K., van Leeuwen, F.N., Middelbeek, J., 2015. Beyond ion-conduction: Channel-dependent and -independent roles of TRP channels during development and tissue homeostasis. Biochim Biophys Acta.
Wang, F.S., Wolenski, J.S., Cheney, R.E., Mooseker, M.S., Jay, D.G., 1996. Function of myosin-V in filopodial extension of neuronal growth cones. Science 273, 660-663.
Wang, Y., Shibasaki, F., Mizuno, K., 2005. Calcium signal-induced cofilin dephosphorylation is mediated by Slingshot via calcineurin. J Biol Chem 280, 12683-12689.
White, D.E., Rayment, J.H., Muller, W.J., 2006. Addressing the role of cell adhesion in tumor cell dormancy. Cell cycle 5, 1756-1759.
Wirtz, D., Konstantopoulos, K., Searson, P.C., 2011. The physics of cancer: the role of physical interactions and mechanical forces in metastasis. Nat Rev Cancer 11, 512-522.
Yang, J., Weinberg, R.A., 2008. Epithelial-mesenchymal transition: at the crossroads of development and tumor metastasis. Dev Cell 14, 818-829.
Yoon, K.J., Danks, M.K., 2009. Cell adhesion molecules as targets for therapy of neuroblastoma. Cancer biology & therapy 8, 306-311.

Figure legends

Figure 1. TRPM7 associates with components of the actomyosin cytoskeleton

A) Flow chart for proteomic analysis of the TRPM7 complex.

B) Detection of TRPM7 associated proteins by silver staining of SDS-PAGE gels. HA-tagged TRPM7 was isolated by immunoprecipitation using anti-HA monoclonal antibodies (12CA5) from N1E-115 control and TRPM7-transduced cells. Proteins were separated by SDS-PAGE on 6% (top) and 12% (bottom) gels and subjected to silver staining. Proteins which co-immunoprecipitating with TRPM7, are indicated.

C. TRPM7-HA immunoprecipitates (IP) are enriched for cytoskeletal proteins. Gene ontology (GO) analysis was performed on the set of proteins exclusively present or enriched (iBAQ > 10) in TRPM7 IP and proteins identified in control IP. GO enrichment, relative to the mouse whole genome, was determined for both IPs. GO terms in categories 'biological process', 'molecular function' and 'cell component', that were most significantly enriched in the TRPM7 IPs, are indicated. The fraction of proteins within the IPs, annotated to these terms, are presented in a bar chart. Statistical significance between control and TRPM7 IP content was determined by a fisher exact test (*** = $p < 0.0001$).

Figure 2. TRPM7 specifically interacts with a cytoskeletal complex

The interactions between TRPM7 and the actomyosin cytoskeleton are specific. Protein complexes were immunoprecipitated from N1E-115 control and TRPM7 overexpressing

cells, using anti-HA antibodies (12CA5). Proteins present in immunoprecipitations (IP, left) and total lysates (TL, right) were detected by Western blot. Known invadosome components are indicated in red.

Figure 3. TRPM7 cytoskeletal interactors localize to invadosomes

By using confocal microscopy, known (myosin IIA) and novel invadosome components were identified in N1E-115 cells that stably overexpress TRPM7. If available, antibody staining was performed (myosin IIA, IIB and IIC, drebrin, $p116^{Rip}$, Tropomodulin2 and α-actinin4). Alternatively, protein localization was evaluated by expression of GPP- or myc-tagged proteins (myosin V and SIPA1-L1). Actin was visualized by Alexa-568 Phalloidin labeling, to indicate invadosome cores (Red). All the tested TRPM7 interactors (green) localized to peripheral invadosomes. Scale bars: 5 μm.

Figure 4. Expression levels of TRPM7 interactome components correlate with disease outcome in a neuroblastoma patient cohorts

A) Overview of TRPM7 interactome components that correlate with overall survival (OS) and recurrence free survival (RFS) in at least two out of three patient datasets (Kocak-649, Versteeg-88 and Oberthuer-251). P-values are corrected for multiple testing (bonferoni and false discovery rate). n.s. = not significant; - = gene not present on array; KM-arm 'low' means that low expression correlates with poor outcome, 'high' means that high expression predicts poor outcome in the Kaplan-Meier analysis. $P < 0.05$ was considered significant.

B) Kaplan-Meier analysis of overall survival according to mRNA expression levels of TRPM7 cytoskeletal interactors. Low expression of *JUP*, *MYL6, MYO5A* in the Kocak-649 patient dataset, and *TMOD2* in the Versteeg-88 patient dataset, strongly correlate with poor disease outcome. P-values are based on log-rank test and corrected for multiple testing (bonferoni).

Table 1. Overview of TRPM7 interactome components and their association with invadosomes and cancer progression

All 64 TRPM7 interactors (iBAQ score > 10) are categorized by general biological function. Components are indicated by protein name, gene symbol and gene ID (for mouse and human). Known (+) and novel invadosome components are indicated, as well as established associations with cancer progression (CA), as was determined by literature search. [1] = associated with neuroblastoma progression.

Table 1

Category	Protein name	Gene Symbol	Gene ID		Invadosome	CA
			Mouse	Human		
Actin Dynamics	Actin, cytoplasmic 1	ACTB	11461	60	+	+
	Actin, cytoplasmic 2	ACTG1	11465	71	+	
	Actin-related protein 2	ACTR2	66713	10097	+	+
	Actin-related protein 2/3 complex subunit 1A	ARPC1A	56443	10552	+	+
	Actin-related protein 2/3 complex subunit 1B	ARPC1B	11867	10095	+	+
	Actin-related protein 2/3 complex subunit 2	ARPC2	76709	10109	+	+
	Actin-related protein 2/3 complex subunit 3	ARPC3	56378	10094	+	
	Actin-related protein 2/3 complex subunit 4	ARPC4	68089	10093	+	
	Actin-related protein 2/3 complex subunit 5	ARPC5	67771	10092	+	+
	Actin-related protein 2/3 complex subunit 5-like protein	ARPC5L	74192	81873	+	
	Cofilin-1	CFL1	12631	1072	+	+
	Drebrin	DBN1	56320	1627	novel	+
	F-actin-capping protein subunit alpha-1	CAPZA1	12340	829		+[1]
	F-actin-capping protein subunit alpha-2	CAPZA2	12343	830		+
	F-actin-capping protein subunit beta	CAPZB	12345	832		
	Gelsolin	GSN	227753	2934	+	+
	Tropomodulin-2	TMOD2	50876	29767		+
	Tropomodulin-3	TMOD3	50875	29766		
	Tropomyosin alpha-1 chain	TPM1	22003	7168	+	+
	Tropomyosin alpha-3 chain, isoform 1 & 2	TPM3	59069	7170	+	+
	Tropomyosin alpha-4 chain	TPM4	326618	7171	+	+
Molecular motors	Myosin light chain 3	MYL3	17897	4634		
	Myosin light chain, regulatory B-like	MYL9	67268	10398		
	Myosin light polypeptide 6	MYL6	17904	4637		
	Myosin-9 (NMHC IIA)	MYH9	17886	4627	+	+
	Myosin-10 (NMHC IIB)	MYH10	77579	4628	novel	
	Myosin-11	MYH11	17880	4629		
	Myosin-14 (NMHC IIC)	MYH14	71960	79784	novel	
	Myosin-Ib	MYO1B	17912	4430		
	Myosin-Ic	MYO1C	17913	4641		
	Myosin-1e	MYO1E	71602	4643		
	Myosin Va	MYO5A	17918	4644	novel	+
	Myosin VI	MYO6	17920	4646		+
Scaffold / Structural protein	Alpha-actinin-4	ATCN4	60595	81	novel	+
	Desmoplakin	DSP	109620	1832		+
	LIM and calponin homology domains-containing protein 1	LIMCH1	77569	22998		
	LIM domain and actin-binding protein 1	LIMA1	65970	51474		+
	Myosin phosphatase Rho-interacting protein	MPRIP/p116RIP	26936	23164	novel	
	Neurabin-2	PPP1R9B	217124	84687		+
	Plectin	PLEC	18810	5339	+	+
Enzymatic activity	Protein phosphatase Slingshot homolog 2	SSH2	237860	85464		
	Signal-induced proliferation-associated 1-like protein 1	SIPA1L1	217692	26037		
	Transient receptor potential cation channel subfamily M member 7	TRPM7	58800	54822	+	+
Other	Annexin A2	ANXA2	12306	302		+
	Calmodulin	CALM1	12313	801		
	Fructose-bisphosphate aldolase A	ALDOA	11674	226		+
	Junction plakoglobin	JUP	16480	3728		+
	Kinase D-interacting substrate of 220 kDa	KIDINS220	77480	57498		+[1]
	Pericentriolar material 1 protein	PCM1	18536	5108		+
	Tax1-binding protein 1 homolog	TAX1BP1	52440	8887		+
Non-cytoskeleton-related	116 kDa U5 small nuclear ribonucleoprotein component	EFTUD2	20624	9343		
	14-3-3 protein sigma	SFN	55948	2810		+[1]
	AT-rich interactive domain-containing protein 1A	ARID1A	93760	8289		+[1]
	ELAV-like protein 3	ELAVL3	15571	1995		
	Histone H3.2	HIST1H3E	319151	8353		
	Importin-7	IPO7	233726	10527		

Importin-9	IPO9	226432	55705	
Prelamin-A/C	LMNA	16905	4000	+
Probable ATP-dependent RNA helicase DDX5	DDX5	13207	1655	+[1]
Protein transport protein Sec16B	SEC16B	89867	89866	
Sarcoplasmic/endoplasmic reticulum calcium ATPase 2	ATP2a2	11938	488	+
Transcription intermediary factor 1-beta	TRIM28	21849	10155	+
Ubiquitin carboxyl-terminal hydrolase 15	USP15	14479	9958	
Voltage-dependent anion-selective channel protein 1	VDAC1	22333	7416	+

Figure 1

A

IP from N1E-115 control and TRPM7-HA overexpressing cells

↓

1D SDS-PAGE (6-12% PAA)

↓

Silver stain gel

↓

In-gel digest with trypsin

↓

Cut gel into 24 pieces

↓

nanoLC-MS/MS

↓

Reverse database search to set false positve rate

↓

Identify enriched proteins:

$$\frac{\text{iBAQ control IP}}{\text{iBAQ TRPM7 IP}} > 10$$

B

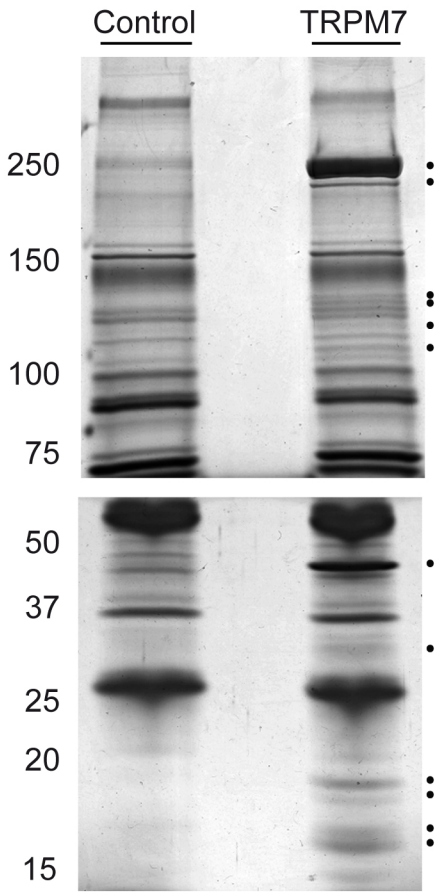

C

	Sample	Fold enrichment
GO Biological process	TRPM7	28.95 ***
Actin filament-based process	Control	3.44
GO Molecular function	TRPM7	27.19 ***
Actin binding	Control	2.55
GO Cell component	TRPM7	33.89 ***
Actin cytoskeleton	Control	3.96

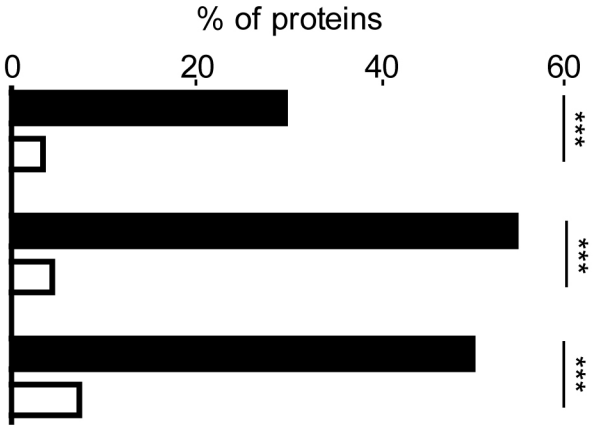

Figure 2

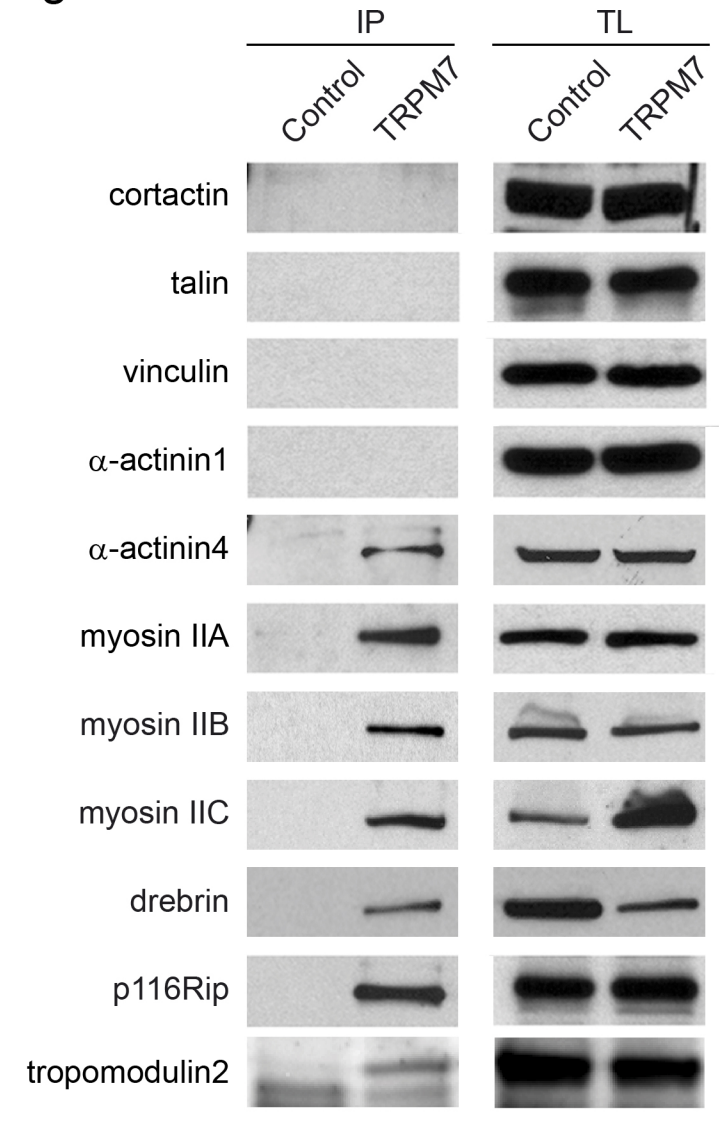
IP
TL
Control
TRPM7
Control
TRPM7
cortactin
talin
vinculin
α-actinin1
α-actinin4
myosin IIA
myosin IIB
myosin IIC
drebrin
p116Rip
tropomodulin2

Figure 3

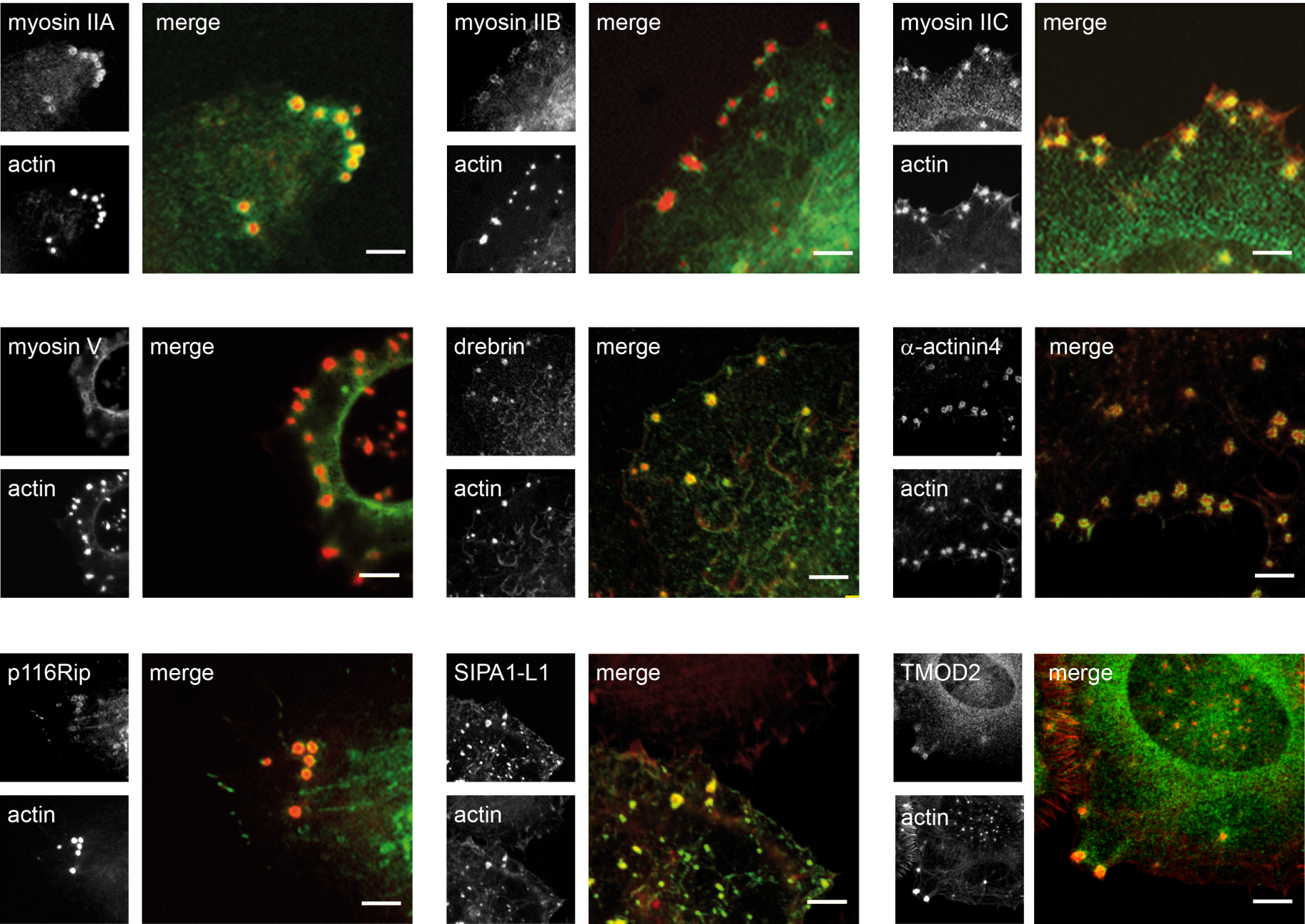
myosin IIA
merge
actin
myosin IIB
merge
actin
myosin IIC
merge
actin
myosin V
merge
actin
drebrin
merge
actin
α-actinin4
merge
actin
p116Rip
merge
actin
SIPA1-L1
merge
actin
TMOD2
merge
actin

Figure 4

A

Gene	KM-arm	Kocak-649		Versteeg-88		Oberthuer-251	
		OS	RFS	OS	RFS	OS	RFS
ACTR2	low	1.10E-03	n.s.	1.90E-04	8.60E-04	-	-
ANXA2	low	1.10E-15	4.70E-09	n.s.	2.10E-02	-	-
ELAVL3	low	7.90E-07	5.10E-05	n.s.	n.s.	7.00E-07	5.90E-06
GSN	low	1.30E-07	1.10E-05	n.s.	n.s.	2.60E-17	6.70E-09
JUP	low	3.90E-17	2.50E-16	-	-	5.10E-09	4.50E-09
KIDINS220	low	7.90E-08	1.20E-05	2.00E-04	2.20E-02	-	-
MYL6	low	7.50E-29	4.50E-14	n.s.	n.s.	6.20E-05	8.20E-05
MYO5A	low	2.40E-11	2.20E-11	1.60E-10	4.10E-06	6.00E-07	1.40E-08
MYO6	low	1.30E-02	n.s.	n.s.	n.s.	3.20E-03	1.10E-02
TAX1BP1	low	1.00E-16	6.50E-16	1.70E-03	1.10E-02	9.70E-14	1.50E-06
TMOD2	low	n.s.	n.s.	6.90E-10	2.40E-05	1.50E-04	1.20E-04
ALDOA	high	n.s.	n.s.	1.40E-02	n.s.	8.30E-03	1.20E-02
DDX5	high	2.90E-03	4.70E-02	2.20E-04	8.10E-04	1.30E-02	n.s.
EFTUD2	high	7.00E-07	1.30E-03	8.50E-07	6.90E-04	-	-
IPO7	high	1.10E-17	7.60E-16	2.90E-04	4.00E-04	n.s.	1.20E-02
TPM3	high	n.s.	3.70E-03	3.10E-03	n.s.	n.s.	n.s.
TPM4	high	4.40E-10	5.60E-11	4.90E-02	2.60E-02	-	-
TRIM28	high	2.70E-13	3.00E-09	1.70E-05	2.40E-03	7.30E-20	9.70E-12

B